

Earth and Space Science



RESEARCH ARTICLE

10.1029/2020EA001142

Key Points:

- A numerical aerosol growth model is developed to consider growth of charged and neutral aerosols
- The model includes terms attributed to the condensation of small ion clusters onto aerosols
- Modeled growth rates are enhanced by ion condensation in agreement with recent experiments

Correspondence to:

J. Svensmark,
jacob.svensmark@nbi.ku.dk

Citation:

Svensmark, J., Shaviv, N. J., Enghoff, M. B., & Svensmark, H. (2020). The ION-CAGE code: A numerical model for the growth of charged and neutral aerosols. *Earth and Space Science*, 7, e2020EA001142. <https://doi.org/10.1029/2020EA001142>

Received 17 FEB 2020

Accepted 18 JUL 2020

Accepted article online 31 JUL 2020

The ION-CAGE Code: A Numerical Model for the Growth of Charged and Neutral Aerosols

J. Svensmark^{1,2} , N. J. Shaviv³ , M. B. Enghoff² , and H. Svensmark² 

¹DARK, Niels Bohr Institute, University of Copenhagen, Copenhagen, Denmark, ²National Space Institute, Danish Technical University, Lyngby, Denmark, ³The Racah Institute of Physics, The Hebrew University of Jerusalem, Jerusalem, Israel

Abstract The presence of small ions influences the growth dynamics of a size distribution of aerosols. Specifically, the often neglected mass of small ions influences the aerosol growth rate, which may be important for terrestrial cloud formation. To this end, we develop the Ion and Charged Aerosol Growth Enhancement (ION-CAGE) code, a numerical model to calculate the growth of a species of aerosols in the presence of charge, which explicitly includes terms for ion condensation. It is shown that a positive contribution to aerosol growth rate is obtained by increasing the ion-pair concentration through this ion condensation effect, consistent with recent experimental findings. The ion condensation effect is then compared to aerosol growth from charged aerosol coagulation, which is seen to be independent of ion-pair concentration. Growth rate enhancements by ion condensation are largest for aerosol sizes less than ~25 nm and increases proportional to the ion concentration. The effect of ion condensation is expected to be most important over pristine marine areas. The model source code is made available through a public repository.

Plain Language Summary It is unresolved whether there is a link between atmospheric ionization from galactic cosmic rays and terrestrial cloud formation. Support for the link is in part based on satellite observations and is further substantiated by recent laboratory experiments, which have detailed a microphysical aerosol mechanism that may give rise to this link. To test whether the mechanism can be the cause of the observed cosmic ray-cloud link, numerical experiments are needed. In this article, we have developed an open-source numerical model that allows for initial numerical experiments of this connection. Using the model, we show that atmospheric ions accelerate the growth of cloud precursor aerosols, which is consistent with the laboratory observations and supports the reality of the cosmic ray-cloud link.

1. Introduction

There is no shortage of numerical models aimed at describing the production, growth, and transport of aerosols for a broad range of parameters, environments, and applications. Often, the scenarios that these models describe turn out very demanding from a computational point of view. Thus, as with any model, a number of optimizations and compromises must be made in terms of included effects and mechanisms, dimensionality, resolution, and so forth. Recent advances in our understanding of the interplay between atmospheric aerosols and electrical charge has heightened the need for aerosol growth modeling that takes charge into account in a detailed way, as charge seems to act as an enhancing agent for aerosol growth rate under atmospheric conditions relevant for marine aerosols (H. Svensmark et al., 2017, hereafter “SESS17 paper”). In order to conduct tests of theoretical assumptions or design and understand future experimental efforts in which charged aerosols are present, a complementary simple, modifiable, open-source numerical model can be helpful. Several advanced models describing aerosol dynamics have been developed, for example, Pierce and Adams (2009), Yu and Turco (2001), Laakso et al. (2002), Kazil and Lovejoy (2004), Leppä et al. (2009), and McGrath et al. (2012). While some of these models take the charge of aerosols into account, none so far study the mechanism of ion-induced condensation, that is, the accelerated growth caused by the mass of ions. Leppä et al. (2009) include charge but do not explicitly model the condensation of ions onto aerosols, and the code is not freely available. Others, such as Prakash et al. (2003), are open source but do not include charge at all.

©2020. The Authors.

This is an open access article under the terms of the Creative Commons Attribution License, which permits use, distribution and reproduction in any medium, provided the original work is properly cited.

In the present work we introduce the Ion and Charged Aerosol Growth Enhancement (ION-CAGE) model: a zero-dimensional box model capable of solving the general dynamics equation (GDE) numerically for both single-charged and neutral aerosol species. Uniquely, this model includes terms considering the addition of the nonzero mass of ions upon interactions with aerosols. It is coded in a way that allows for the easy inclusion or exclusion of a selection of the usual GDE terms, as well as code structure that can easily be modified to include new terms where desired. For this work the model is set up to simulate the growth of sulfuric acid aerosols in an environment corresponding to clean marine air, as relevant for the SESS17 experiment. The numerical solutions involving ion accelerated growth of aerosols demonstrate excellent agreement with the SESS17 theoretical results. To further test the theory, it would be useful to incorporate it into more advanced models, like those mentioned above. However, the results presented here already make it feasible to test the SESS17 theory in computationally heavy global circulation models.

In the following sections we present the terms of the GDE that are included in the model and demonstrate that it operates in correspondence with expectations. We apply the model by reproducing and expanding on the results of the SESS17 paper, by probing the growth rate of aerosols exposed to varying concentrations of ions pairs and aerosols, considering also aerosol coagulation.

2. Model Overview

The ION-CAGE model considers the temporal evolution of number concentrations for the following species: Neutral and charged small stable and condensable molecular clusters (henceforth “neutral clusters” and “ions,” respectively) and neutral and singly charged aerosols of both signs. Ions and neutral clusters are set at a certain diameter and number density, whereas the aerosols exist at a number N_{tot} of logarithmically spaced nodes in volume as indicated by the index $k \in [1, N_{\text{tot}}]$. This helps the model span the several orders of magnitude in volume that corresponds to aerosol diameters of typically between 1 and 100 nm. Given a set of initial conditions for a distribution of neutral clusters, ions, and aerosols along all volume nodes, as well as interaction coefficients, production and loss parameters, and other relevant inputs (see below for all parameters), the initial distribution is propagated through forward integration of the GDE using a fourth-order Runge-Kutta algorithm (Fehlberg, 1969; Shampine et al., 1976). As shall be explored below, the GDE contains terms describing the nucleation of new aerosols, the condensation of neutral clusters and ions onto the aerosols, and the coagulation of two aerosols into a single larger aerosol and production and loss terms all while keeping track of the exchange of charge between all species, except between neutral clusters and ions. Importantly, the mass of the ion can be taken into account such that its small but important contribution to the condensation term is included. The model is written in the FORTRAN language, and its source code as used in this paper is downloadable from a public repository (Svensmark zenodo, <https://doi.org/10.5281/zenodo.3931374>). The code is maintained at GitHub (<https://github.com/jacobsvensmark/ioncage>).

2.1. Size Nodes

To create a set of N_{tot} volume nodes v_k distributed linearly in logarithmic space between two volumes v_{min} and v_{max} , we use the following:

$$v_k = 10^{\frac{\log(v_{\text{min}}) + \frac{k-1}{N_{\text{tot}}-1}(\log(v_{\text{max}}) - \log(v_{\text{min}}))}{1}}, \quad (1)$$

where k is an integer between 1 and N_{tot} (see Table 1 for list of variables). In this way two neighboring nodes are separated by a factor C such that $v_k = Cv_{k-1}$. Aerosols in the model have a charge of $q = [0, -, +]$, that is, 0, -1 , or 1 elementary charge. The concentration of aerosols at volume v_k and charge q is denoted N_k^q , and thus, the model keeps track of $3N_{\text{tot}}$ aerosol concentrations. A diagram of the node structure can be seen in Figure 1. Additionally, the model has neutral condensable clusters at concentration n^0 , as well as condensable positive and negative ions at concentrations n^+ and n^- , all of which we refer to as monomers. These concentrations constitute the state of the model, and following a set of terms that make up the GDE of this model, the state is propagated forward in time. The terms that govern the dynamics of this process are presented in the next section.

3. Interactions

In the following we formulate the interactions governing the temporal derivatives between charged and neutral aerosols, ions, and neutral condensable clusters.

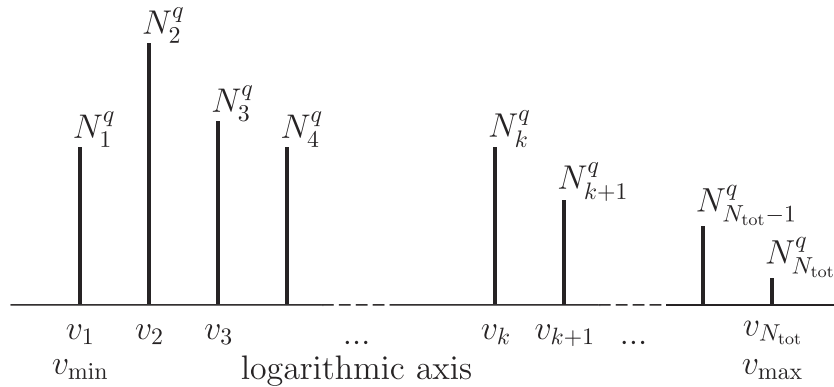


Figure 1. Overview of the node structure of the volume bins and the concentrations at each node for a given charge q . Note that the scale is logarithmic, that each node is a factor of C larger than its smaller neighbor: $v_k = Cv_{k-1}$.

A diagram showing the condensation and coagulation rules can be seen in Figure 2. Since the sizes of the aerosols of interest are typically in the range 1–100 nm, only singly charged aerosols are considered. In-depth discussions on the information presented here can be found in, for example, Seigneur et al. (1986), Y. Zhang et al. (1999), and Seinfeld and Pandis (2006).

The overall dynamical equations for aerosols at charge $q = [0, -, +]$ are

$$\frac{dN_k^q}{dt} = \left[\frac{dN_k^q}{dt} \right]_{\text{nucleation}} + \left[\frac{dN_k^q}{dt} \right]_{\text{condensation}} + \left[\frac{dN_k^q}{dt} \right]_{\text{coagulation}} + \left[\frac{dN_k^q}{dt} \right]_{\text{loss}}. \quad (2)$$

The first term on the right-hand side of Equation 2 contains a simple contribution to the nucleation of new aerosol particles of charge $q = [0, -, +]$. The second contains the condensation of neutral clusters and ion mass onto aerosols while keeping track of the charge of the aerosols in this process. The third term is the most computationally expensive term and describes the coagulation of two aerosols into a larger common aerosol, again taking charge into account. The fourth and final term adds losses in the form of scavenging by large particles and losses to walls required for modeling an experimental situation.

Similarly for the neutral cluster and ion concentrations n^q , the terms of the overall GDE are

$$\frac{dn^q}{dt} = \left[\frac{dn^q}{dt} \right]_{\text{nucleation}} + \left[\frac{dn^q}{dt} \right]_{\text{condensation}} + \left[\frac{dn^q}{dt} \right]_{\text{production}} + \left[\frac{dn^q}{dt} \right]_{\text{loss}}. \quad (3)$$

Here the first and second terms on the right-hand side describe the same processes as those of Equation 2. The third term includes production of monomers, and the final loss term takes ion recombination into account in addition to wall losses. The number of coupled equations becomes $3N_{\text{tot}} + 3$, where the

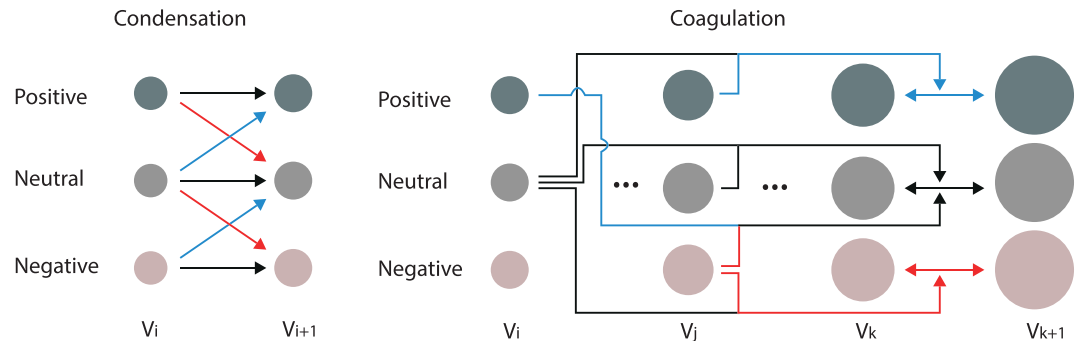


Figure 2. Diagram showing how condensation (left) and coagulation (right) transports. For the condensation, the charge of the condensing element is symbolized by the color of arrow (red for negative, black for neutral, and blue for positive). For the coagulation, the joint volume of aerosols v_i and v_j is split between node at volume v_k and v_{k+1} taking charge into account.

numbers three denote the three charging states of the aerosols and three rate equations for neutral clusters and ions. The code is written in a modular form to allow easy modification, expansion, or decoupling of each of the terms.

3.1. Nucleation

A nucleation term specifies the amount of new aerosols generated per unit time at a specified critical volume v_*^q , where $q = [0, -, +]$ denotes the charge. The production of new aerosols at this size is set to a fixed rate J^q . The volume of the nucleated particles may fall in between two nodes or below the lowest node. Following the design of Prakash et al. (2003), the number concentration is then scaled by volume and placed in the node immediately above it, such that

$$\left[\frac{dN_k^q}{dt} \right]_{\text{nucleation}} = \begin{cases} J^q \frac{v_*^q}{v_1}, & \text{for } v_*^q \leq v_1 \\ J^q \frac{v_*^q}{v_k}, & \text{for } v_{k-1} < v_*^q \leq v_k \\ 0, & \text{otherwise.} \end{cases} \quad (4)$$

Once ion nucleation is applied, it is important to maintain charge conservation. Positively and negatively nucleated aerosols take their charge from the ions in a number corresponding to what was nucleated at the critical volume, and this charge has to be subtracted from the positive and negative ion equations, that is,

$$\begin{aligned} \left[\frac{dn^-}{dt} \right]_{\text{nucleation}} &= -J^-, \\ \left[\frac{dn^+}{dt} \right]_{\text{nucleation}} &= -J^+. \end{aligned} \quad (5)$$

This simplistic view on aerosol nucleation is easily expanded. The nucleation could be modified to depend on other quantities in the model such as neutral cluster and ion concentrations, temperature, and/or further parametrization (Dunne et al., 2016; Määttä et al., 2018; Yu, 2010).

3.2. Condensation

Three channels of condensation of clusters onto aerosol particles are allowed: neutral clusters of concentration n^0 condensing onto all aerosols and two classes of ions n^+ and n^- with a single charge condensing onto neutral aerosols or aerosols of opposite sign. Schematically, we write

$$\left[\frac{dN_k^q}{dt} \right]_{\text{condensation}} = \left[\frac{dN_k^q}{dt} \right]_{\text{cond}, n^0} + \left[\frac{dN_k^q}{dt} \right]_{\text{cond}, n^+} + \left[\frac{dN_k^q}{dt} \right]_{\text{cond}, n^-}, \quad (6)$$

where $q = [0, -, +]$ indicates the neutral, positive, and negative charges, respectively. This yields three equations of three terms summarized in the following equation:

$$\left[\frac{dN_k^q}{dt} \right]_{\text{condensation}} = - \sum_p I_k^{qp} N_k^p + \sum_p I_{k-1}^{qp} N_{k-1}^p, \quad (7)$$

where

$$I_k^{qp}(r, t) = \begin{pmatrix} A_k^0 n^0 \beta_k^{00} & A_k^+ n^+ \beta_k^{+-} & A_k^- n^- \beta_k^{-+} \\ A_k^- n^- \beta_k^{-0} & A_k^0 n^0 \beta_k^{0-} & 0 \\ A_k^+ n^+ \beta_k^{+0} & 0 & A_k^0 n^0 \beta_k^{0+} \end{pmatrix}. \quad (8)$$

For an aerosol to grow from volume v_k to v_{k+1} , a number $(v_{k+1} - v_k)/v^q$ of condensing monomers of volume v^q are needed. The coefficients $A_k^q = v^q/(v_{k+1} - v_k)$ are thus the fractional volume that one condensing monomer contributes to growing an aerosol from volume v_k to v_{k+1} . This is analogous to the treatment of condensation in, for example, Prakash et al. (2003). q and p indicate the charge, and the β_k^{qp} denotes the interaction coefficient between a monomer (neutral or ion) of charge $q = [0, -, +]$ and an aerosol at size node k and charge $p = [0, -, +]$. The diagonal elements account for the usual condensation of neutral clusters,

Table 1

Table With Variables and Their Descriptions Used in the Present Paper

Symbol	Unit	Description
v_k	m^3	Volume of aerosol node k
v^q	m^3	Volume of monomer of charge q
v_{min}	m^3	Volume of the smallest node
v_{max}	m^3	Volume of the largest node
v_*^q	m^3	Critical volume at which nucleation takes place for aerosols at charge q
t	s	Time
C		Ratio between volumes of two neighboring nodes
N_{tot}		Number of logarithmically spaced size nodes
q, p		Indices specifying charge may be (0, −, +) dictating negative, neutral, and positive charge, respectively.
i, j, k		Indices specifying node number
σ		Index with values 1,2,3,4
N_k^q	m^{-3}	Particle concentration of particles at node number k and charge q
N_L	m^{-3}	Concentration of large mode aerosols used in scavenging loss term
n^q	m^{-3}	Concentrations of neutral ($q = 0$) or ion monomers ($q = -$ or $q = +$)
J^q	$\text{m}^{-3} \text{s}^{-1}$	Nucleation rate of charged or neutral aerosols.
β_k^{qp}	$\text{m}^3 \text{s}^{-1}$	Condensation coefficient of interactions between a monomer of charge q and an aerosol of charge p at size node k
$\kappa_{i,j}^{qp}$	$\text{m}^3 \text{s}^{-1}$	Coagulation coefficient of interactions between an aerosol from size node i and charge q , and another aerosol from size node j and charge p
β_L^{q0}	$\text{m}^3 \text{s}^{-1}$	Condensation coefficient for loss of monomers of charge q onto large mode scavenging aerosols
$\kappa_{k,L}^{q0}$	$\text{m}^3 \text{s}^{-1}$	Coagulation coefficient for losses of an aerosol from size node k and charge q , and a large mode scavenging aerosol
$S_{i,j}$		Splitting matrix denoting the fractional contribution of two coagulating particles from node i and j to two neighboring nodes
P	$\text{m}^{-3} \text{s}^{-1}$	Neutral cluster production rate
Q	$\text{m}^{-3} \text{s}^{-1}$	Ion-pair production rate
α	$\text{m}^3 \text{s}^{-1}$	Recombination coefficient
d	m	Aerosol diameter

while the other four nonzero elements make up the terms related to the condensation of ions. The 0 terms in the matrix represent the negligible interactions between like-charged ions and aerosols.

As monomers condense onto the aerosols, neutral cluster and ion concentrations change accordingly:

$$\begin{aligned}
 \left. \frac{dn^0}{dt} \right|_{\text{condensation}} &= -n^0 \sum_{k=1}^{N_{\text{tot}}} (\beta_k^{00} N_k^0 + \beta_k^{0+} N_k^+ + \beta_k^{0-} N_k^-), \\
 \left. \frac{dn^-}{dt} \right|_{\text{condensation}} &= -n^- \sum_{k=1}^{N_{\text{tot}}} (\beta_k^{-0} N_k^0 + \beta_k^{-+} N_k^+), \\
 \left. \frac{dn^+}{dt} \right|_{\text{condensation}} &= -n^+ \sum_{k=1}^{N_{\text{tot}}} (\beta_k^{+0} N_k^0 + \beta_k^{+-} N_k^-).
 \end{aligned} \tag{9}$$

The code can easily switch on/off the terms related to the usual condensation and ion condensation separately. The reverse process, loss of aerosol volume due to evaporation, is not implemented in the present

model since only stable clusters are considered. Note that evaporation is not needed for demonstrating the novel feature of ion condensation. It is straightforward to include evaporation as a future extension of the model.

3.3. Monomer Production

A term describing the production of the monomers is included in the model in the following simple way:

$$\left. \frac{dn^0}{dt} \right]_{\text{production}} = P, \quad (10)$$

$$\left. \frac{dn^-}{dt} \right]_{\text{production}} = Q, \quad (11)$$

$$\left. \frac{dn^+}{dt} \right]_{\text{production}} = Q. \quad (12)$$

Here, P is the production rate of the neutral cluster elements n^0 , and Q is the ion-pair production rate. Both rates are input to the model as constants but can easily be generalized to describe more advanced cases. The code allows for bypassing the production rates to keep a constant concentration of any of the n^q . Note that the production of monomers is a term different from the nucleation term: Production is the process with which monomers is introduced into the model. Nucleation is the process where monomers join to become stable aerosols.

3.4. Coagulation

When particles of volume v_i and v_j coagulate, they produce a new particle with a volume $v_i + v_j$, which may in general lie between two nodes k and $k + 1$. Thus, the coagulated volume needs to be split and distributed between N_k^q and N_{k+1}^q . To do so, we calculate a matrix giving for each i, j pair the index k of the node immediately below the new coagulated volume:

$$V_{ij} = f_k(v_i + v_j) = \text{floor} \left[N_{\text{tot}} \left(\frac{\log(v_i + v_j) - \log v_{\min}}{\log v_{\max} - \log v_{\min}} \right) \right]. \quad (13)$$

v_{\min} is the volume of the smallest node and v_{\max} that of the largest. We also calculate a splitting fraction function

$$f_s(v) = \frac{v_{k+1} - v}{v_{k+1} - v_k}, \quad (14)$$

where $f_s(v)$ is a function giving the volume fraction added to node $k = f_k(v)$ while $1 - f_s(v)$ is added to node $k + 1$. The function $f_s(v)$ is defined such that $v = f_s(v_k)v_k + (1 - f_s(v_k))v_{k+1}$, implying that the total volume is conserved with this definition of splitting.

To save computing time, a splitting matrix is calculated during initialization and used throughout the calculation. Its terms are

$$S_{ij} = f_s(v_i + v_j) = \frac{v_{k+1} - (v_i + v_j)}{v_{k+1} - v_k}. \quad (15)$$

The charge gives rise to four types of coagulation between the aerosols: neutral with neutral, positive with neutral, neutral with negative, and positive with negative. These have four corresponding coagulation coefficient matrices: $\kappa_{ij}^{00}, \kappa_{ij}^{+0}, \kappa_{ij}^{0-}, \kappa_{ij}^{+-}$, each of dimension $N_{\text{tot}} \times N_{\text{tot}}$. Coagulation of like-signed aerosols is neglected, as the model only incorporates single-charge species. During one time step, we can then calculate the interaction terms from each coagulation contribution:

$$\tilde{I}_{ij}^{\sigma} = \begin{pmatrix} I_{ij}^{00} \\ I_{ij}^{+0} \\ I_{ij}^{0-} \\ I_{ij}^{+-} \end{pmatrix} = \begin{pmatrix} \kappa_{ij}^{00} N_i^0 N_j^0 \\ \kappa_{ij}^{+0} N_i^+ N_j^0 \\ \kappa_{ij}^{0-} N_i^0 N_j^- \\ \kappa_{ij}^{+-} N_i^+ N_j^- \end{pmatrix}. \quad (16)$$

The rules for mapping coagulation of two particles of given charges into its electrically relevant node are summarized by the following three matrices:

$$K^{q\sigma} = \begin{pmatrix} \frac{1}{2} & 0 & 0 & 1 \\ 0 & 0 & 1 & 0 \\ 0 & 1 & 0 & 0 \end{pmatrix}, \quad L^{q\sigma} = \begin{pmatrix} -\frac{1}{2} & 0 & -1 & 0 \\ 0 & 0 & 0 & 0 \\ 0 & -1 & 0 & -1 \end{pmatrix}, \quad M^{q\sigma} = \begin{pmatrix} -\frac{1}{2} & -1 & 0 & 0 \\ 0 & 0 & -1 & -1 \\ 0 & 0 & 0 & 0 \end{pmatrix}. \quad (17)$$

As before, q denotes the charge of the end product, and σ is a number between 1 and 4 denoting one of the four possible types of coagulation.

As aerosols at size node i coagulate with those at node j , and distribute their joined volume between node k and $k+1$, where k is a function of i and j , the rate of change in the four nodes is as follows:

$$\begin{aligned} \left. \frac{dN_k^q}{dt} \right|_{\text{coag}} &= S_{ij} \sum_{\sigma} K^{q\sigma} \tilde{T}_{ij}^{\sigma}, \\ \left. \frac{dN_{k+1}^q}{dt} \right|_{\text{coag}} &= (1 - S_{ij}) \sum_{\sigma} K^{q\sigma} \tilde{T}_{ij}^{\sigma}, \\ \left. \frac{dN_i^q}{dt} \right|_{\text{coag}} &= \sum_{\sigma} L^{q\sigma} \tilde{T}_{ij}^{\sigma}, \\ \left. \frac{dN_j^q}{dt} \right|_{\text{coag}} &= \sum_{\sigma} M^{q\sigma} \tilde{T}_{ij}^{\sigma}. \end{aligned} \quad (18)$$

Repeating this for all combinations of i and j yields the total coagulation term. All coagulation channels are covered within the four terms of Equation 16 as the summation runs through all combinations of i and j . The neutral-neutral interactions, however, are counted twice since, for example, the coagulation for $i=1$ and $j=2$ represents the same process as $i=2$ and $j=1$ if both particles are neutral. This is compensated for by the factor of $\frac{1}{2}$ on all neutral-neutral coagulation terms from the matrices of Equation 17.

3.5. Loss Terms

When simulating an experimental situation where an atmospheric reaction chamber is used, loss of aerosols to the walls may be of importance. To accommodate this, a size-dependent loss on N_k^q , n^{\pm} , and n_0 is added to the model. An example of such a loss term was found empirically to depend on aerosol diameter as $dN_k/dt = -\lambda(d/d_0)^{-\gamma}N_k$, where $\gamma = 0.69$ and $\lambda = 6.2 \times 10^{-4} \text{ s}^{-1}$ and $d_0 = 2 \text{ nm}$, for an 8 m^3 reaction chamber (H. Svensmark, et al., 2013). Furthermore, we include losses to large aerosols at concentration N_L and diameter d_L . Extending this to charged aerosols and monomers, the wall loss term can be written for the aerosols as

$$\left. \frac{dN_k^q}{dt} \right|_{\text{loss}} = -\lambda \left(\frac{d_k}{d_{\text{loss}}} \right)^{-\gamma} N_k^q - N_k^q \kappa_{kL}^{q0} N_L, \quad (19)$$

where $d_{\text{loss}} = 2 \text{ nm}$ and d_k is the diameter corresponding to volume node k , and κ_{kL}^{q0} is the coagulation coefficient between the k th aerosol of charge q and the large aerosol. For the monomers we have

$$\left. \frac{dn^q}{dt} \right|_{\text{loss}} = -\lambda \left(\frac{d^q}{d_{\text{loss}}} \right)^{-\gamma} n^q - n^q \beta_L^{q0} N_L + \left. \frac{dn^q}{dt} \right|_{\text{recomb}}, \quad (20)$$

where d^q are the diameters of the monomers and β_L^{q0} is the interaction coefficient between the k th aerosol of charge q and the large aerosol. Here λ , γ , d_{loss} , d_L and N_L , and the coefficients β_k^{qp} and κ_{ij}^{qp} serve as inputs to the model. The losses due to ion-ion recombination are implemented through the recombination coefficient α , such that the recombination term in Equation 20 contains

$$\left. \frac{dn^-}{dt} \right|_{\text{recomb}} = -\alpha n^- n^+, \quad (21)$$

$$\left. \frac{dn^+}{dt} \right|_{\text{recomb}} = -\alpha n^- n^+, \quad (22)$$

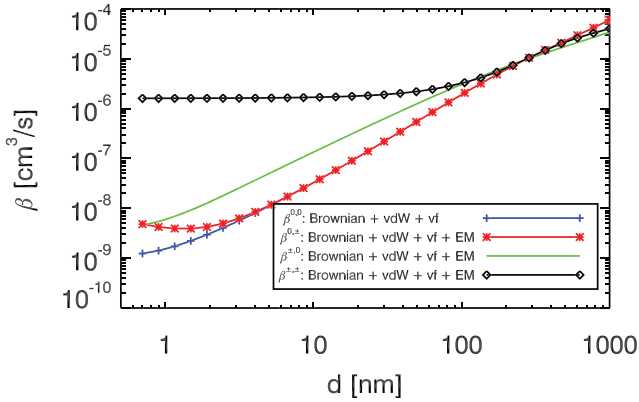


Figure 3. The condensation coefficients β for a neutral cluster monomer or charged ion interacting with aerosols. The potentials are: vdW: van der Waals potential. vf: viscous forces. EM: electrostatic potential. The neutral clusters are here H_2SO_4 and are assumed to have a mass of 100 AMU. Ions have masses of 225 AMU.

species that are modeled and the environment they exist in. We model the interaction caused by condensation of hydrated sulfuric acid clusters onto sulfuric acid-water-aerosols and ions in later parts of the present work. To do that, we model neutral clusters, ions, and aerosols as electrostatically interacting spheres including their image induction in one another. Furthermore van der Waals forces, viscous forces, and dipole moment of the sulfuric acid population are included along with Brownian coagulation to make up the coefficients β . Further information on how the coefficients have been calculated can be found in Appendix A1. Figure 3 displays the β coefficients as a function of aerosol diameter. The choice of parameters for this figure is $m^0 = 100$ AMU, $m^+ = m^- = 225$ AMU to match theoretical assumptions of SESS17, and densities are set to $\rho^0 = \rho^+ = \rho^- = 1,200$ kg m $^{-3}$ (Figure 10.13 of Seinfeld & Pandis, 2006). This models the behavior of hydrated sulfuric acid clusters, ions, and aerosols at 300 K. These coefficients are used throughout the paper, unless otherwise is explicitly stated. The model takes condensation and coagulation coefficient tables as input prior to any calculations, and thus, any relevant coefficients may be provided.

4. Benchmarking the Model

To validate the model, we test whether it can reproduce known solutions to the GDE for simple initial conditions. Thus, a number of benchmark tests are performed. First, a visual representation of the model output is shown in Figure 4. In this example the model was initiated with a steady state distribution. Then, after 8 hr the nucleation rate was increased by a factor of 2 along with a change in the ion-pair production rate from 16 to 500 cm $^{-3}$ s $^{-1}$. After eight additional hours the ion-pair production and nucleation rate was stepped back down, and this process was repeated five times. The figure displays in the first panel the distribution for all aerosols (i.e., $N_k^0 + N_k^+ + N_k^-$) as a function of time. In the lower panels are the neutral, positive, and negative aerosols only also as a function of time. In all figures a clear growth profile is seen with a period of 16 hr; however, significant numerical diffusion affects the simulation for higher radii.

4.1. Testing Condensation and Coagulation

To see that the condensation mechanism is on par with expectations, a known distribution of aerosols is propagated forward in time while neglecting all contributions to the GDE other than the condensation term. The numerical model output can then be compared to an analytic temporal evolution of the same initial conditions. The condensation equation can be written as

$$\frac{\partial n(d, t)}{\partial t} + \frac{A}{d} \frac{\partial n(d, t)}{\partial d} = \frac{A}{d^2} n(d, t) \quad (24)$$

where $A = 4D_i M_i (p_i - p_{\text{eq},i}) / RT \rho_p$ is a constant. An initial continuous lognormal aerosol distribution

$$n(d, 0) = \frac{N_0}{\sqrt{2\pi d \ln \sigma_g}} \exp\left(-\frac{\ln^2(d/D_g)}{2\ln^2 \sigma_g}\right) \quad (25)$$

$$\left. \frac{dn^0}{dt} \right|_{\text{recomb}} = 0. \quad (23)$$

This means that recombining ions effectively disappear from the model. Note that the recombination coefficient $\alpha = 1.6 \times 10^{-6}$ cm 3 s $^{-1}$ is used and set as a constraint on the coefficients β_k^{qp} and κ_{ij}^{qp} we use for demonstration purposes here (see section on parameters and Appendix A1). Condensation of monomers onto aerosols in the largest size node is also lost from the model. Coagulation of an aerosol pair outside the range spanned by the size nodes has their joint volume split according to the splitting matrix in Equation 15, and the upward moving fraction is lost. Other types of loss such as rain out could be added in the code.

3.6. Parameters

To accurately simulate the interactions of aerosols through the channels mentioned above, the interaction coefficients β_k^{qp} and κ_{ij}^{qp} must be described as accurately as possible. These interactions depend on the

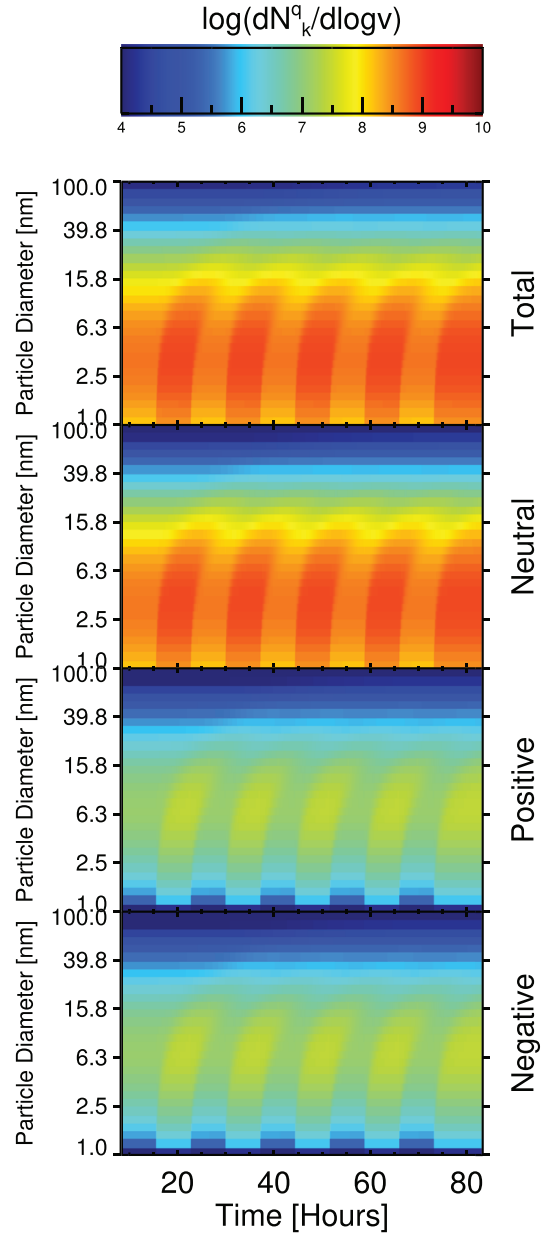


Figure 4. Sixteen hour cycles of neutral aerosol nucleation rate $J^0 = 0.1 \text{ cm}^{-3} \text{ s}^{-1}$ and $J^0 = 0.2 \text{ cm}^{-3} \text{ s}^{-1}$, with ionization rates also alternating between $Q = 16 \text{ cm}^{-3} \text{ s}^{-1}$ and $Q = 500 \text{ cm}^{-3} \text{ s}^{-1}$. Coagulation is not included for this particular calculation.

is grown using only the condensation section of the model (see e.g., Seinfeld & Pandis, 2006, Equation (13.26)). Here N_0 is the number of aerosols, while D_g and σ_g determine the shape of the distribution. Analytically, this solves to

$$n(d, t) = \frac{d}{(d^2 - 2At)} \frac{N_0}{\sqrt{2\pi d} \ln \sigma_g} \exp\left(-\frac{\ln^2[(d^2 - 2At)^{1/2}/D_g]}{2\ln^2 \sigma_g}\right). \quad (26)$$

In Figure 5, the analytical solution as well as a corresponding simulation is seen for the parameters, that is, interaction coefficients written in the figure caption. As can be seen, the peak of the distribution follows the analytical form as expected; however, as the number of volume nodes decreases, the numerical diffusion becomes more apparent. The significant numerical diffusion notably becomes an issue for low number of

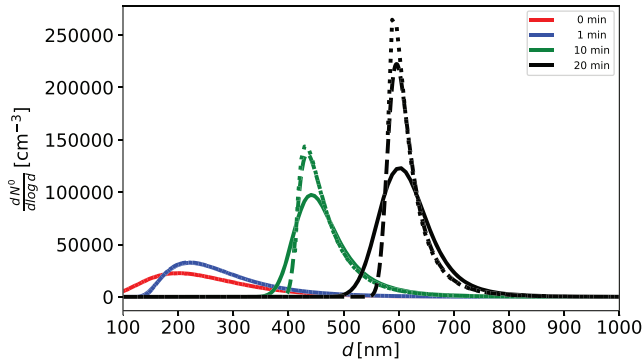


Figure 5. Pure condensation for an initial lognormal distribution of aerosols from Equation 25, using $\sigma_g = 1.5$, $D_g = 200 \times 10^{-9}$ m, and $N_0 = 10,000 \text{ cm}^{-3}$. The condensation coefficients used for this reflect the choice of $(p_i - p_{i,eq}) = 10^{-9}$ atm, $M_i = 100$ g/mol, $D_i = 10^{-5} \text{ m}^2 \text{ s}^{-1}$, $T = 300$ K, $\rho_p = 1.2 \text{ g cm}^{-3}$. Dotted lines show the analytical solution, solid lines are snapshots from a condensation-only simulation, and dashed lines are a similar simulation with a factor of 10 higher density of volume nodes, lowering the numerical diffusion at a high cost in computation. For the solid lines, two adjacent nodes are a factor of 1.013 apart.

nodes, and as such direct implementation of the present algorithm in larger-scale atmospheric models will be difficult due to computational cost. Here, moving center or two-moment methods could be considered.

We will now test the coagulation. The coagulation equation (Equation 13.72 of Seinfeld & Pandis, 2006), for a constant coagulation coefficient $\kappa_k^{qp} = K$ and initial continuous distribution

$$n(v, 0) = \frac{N_0^2}{V_0} \exp\left(\frac{-vN_0}{V_0}\right) \quad (27)$$

solves to

$$n(v, t) = \frac{N_0^2}{V_0(1 + t/\tau_c)^2} \exp\left(-\frac{vN_0}{V_0(1 + t/\tau_c)}\right). \quad (28)$$

Note that now n is a function of aerosol volume v . The characteristic time $\tau_c = 2/(KN_0)$, N_0 is the number concentration of particles at the onset of the calculation or simulation, and V_0 is total volume concentration. The above analytic solution is compared with the numerical solution in Figure 6, left panel. The black lines show the particle spectrum for $t = 0$ as calculated by Equation 28, and the black symbols show the simulated aerosol spectrum at the same instant. The red line and red symbols are

the analytic and numerical solution evolved over $t = 12$ hr. The behavior of the simulated spectra is seen to follow closely that of the analytic ones. It should be noted, however, that as time progresses the largest particles coagulate beyond the upper size node, and as such the volume of simulated coagulation is not strictly conserved. This manifests itself as slight deviations from the analytic solutions toward the high end of the spectrum and worsens as time progresses.

4.2. Charge Distribution in Steady State

A good benchmark for an aerosol model that handles charge is that the charged fractions of aerosols at a given volume node meet analytic expectations. The fraction of charged aerosols in a steady state scenario depends on the coefficients chosen for ion and aerosol interactions. These in turn are affected by a number of parameters, of which some are the ion masses. The ratio of the charged to neutral aerosol concentrations at a given volume node at steady state can be expressed as

$$\frac{N_k^+}{N_k^0} = \frac{n^+ \beta_k^{+0}}{n^- \beta_k^{-+}}, \quad (29)$$

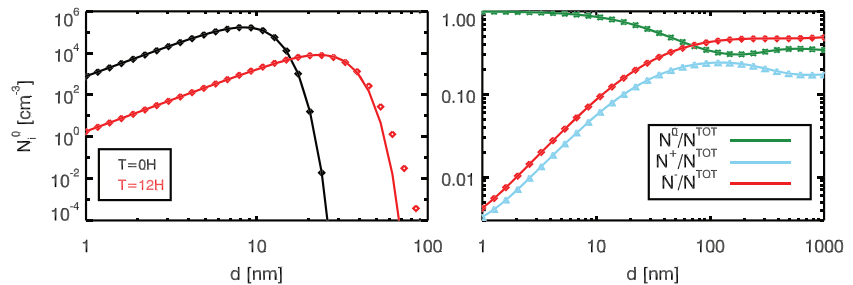


Figure 6. (left) The particle spectrum initially (black) and after 12 hr of simulation for a distribution of the form Equation 28 subject to coagulation only, with a constant coagulation coefficient $K = 10^{-15} \text{ cm}^3 \text{ s}^{-1}$. It can be noted that the analytic and model distributions begin to deviate for larger aerosol diameters as time progresses. This is an effect of the logarithmic spacing of the size nodes, as can be seen also in Figure 15.2 of Jacobson (2005). (right) Fraction of neutral, positively charged, and negatively charged aerosols relative to the total number, as calculated by the model run in steady state (points) and calculated analytically (lines). The plotted quantities are shown in the legend, and that the y axis is unitless. In this particular model run, the mass of the ions is deliberately very different for demonstration purposes: The mass of the neutral monomer is 100 AMU, positive ion is 325 AMU, and negative ion is 150 AMU. These masses are also reflected in the interaction coefficients, which is directly pronounced in the positive and negative aerosol fraction.

$$\frac{N_k^-}{N_k^0} = \frac{n^- \beta_k^{-0}}{n^+ \beta_k^{+-}}, \quad (30)$$

which depends only on ion concentrations and condensation coefficients (Hoppel, 1985). If $N_k^{\text{tot}} = N_k^0 + N_k^+ + N_k^-$, then the above equations solve to

$$\begin{aligned} \frac{N_k^0}{N_k^{\text{tot}}} &= \left(1 + \frac{n^- \beta_k^{-0}}{n^+ \beta_k^{+-}} + \frac{n^+ \beta_k^{+0}}{n^- \beta_k^{-+}} \right)^{-1}, \\ \frac{N_k^+}{N_k^{\text{tot}}} &= \left(1 + \frac{n^- \beta_k^{-+}}{n^+ \beta_k^{+0}} \left(1 + \frac{n^- \beta_k^{-0}}{n^+ \beta_k^{+-}} \right) \right)^{-1}, \\ \frac{N_k^-}{N_k^{\text{tot}}} &= \left(1 + \frac{n^+ \beta_k^{+-}}{n^- \beta_k^{-0}} \left(1 + \frac{n^+ \beta_k^{+0}}{n^- \beta_k^{-+}} \right) \right)^{-1}. \end{aligned} \quad (31)$$

As an illustration, different condensation coefficients are chosen by setting the neutral monomer mass to 100 AMU, positive ion mass to 325 AMU, and negative ion to 150 AMU (as opposed to later, where positive and negative ion masses are assumed equal). The model is then run into a steady state. The continuous lines of Figure 6 in the lower right hand panel show the analytic charge fractions given by Equation 31 as a function of aerosol diameter. The modeled charged aerosol fractions are shown as the diamond symbols and demonstrate a good agreement between the analytical and modeled solutions. The model also reproduces the common observation that aerosols generally have a higher negative than positive charging state, due to differences in ion size and thus mobility (Enghoff & Svensmark, 2017; Wiedensohler, 1988), although the choice of masses in the present example may exaggerate this effect. Note that for larger aerosols (above ~ 100 nm) multiple charging starts to be relevant even though it is not included in the model. In cases with large number of >100 nm aerosols this would begin to impact the amount of available small ions. For most atmospherically relevant situations this will not be a significant issue.

5. Case Study: Simulated Ion-induced Condensation

One of the core features of the model presented in this work is the inclusion of the GDE terms describing ion induced condensation. It is of natural interest to quantify how this growth channel compares to neutral condensation, and this has indeed already been done in SESS17 taking a theoretical and experimental approach. Here it was shown that ion condensation can be an important addition to the neutral condensation growth of aerosols under atmospheric conditions. It was found that the addition of small concentrations of ions relative to the neutral condensable clusters heightened the probability of small nucleated aerosols surviving to cloud condensation nuclei (CCN) sizes >50 nm, which will have an impact on cloud microphysics in the terrestrial atmosphere. The strength of the theoretical ion condensation description is that it shows how the ions contribution to growth rate is independent of aerosol size distribution. This description however neglects growth from coagulation, which may also be affected by the presence of ions. While the theoretical result of SESS17 is consistent with the experimental findings of the same paper, it is interesting to expand on aerosol growth from ion induced condensation in the context of neutral and charged coagulation. In order to do so, we first reconsider the theoretical description of aerosol growth in the context of charge. Our focus will lie on the growth rate

$$GR = \frac{d}{dt} \quad (32)$$

of aerosols at diameter d and explore the conditions under which ion-induced condensation can be said to be important.

5.1. Condensation Growth Rate

In the case of purely neutral condensation, the growth rate can be written as

$$GR_{\text{cond}}^0 = A_0 n^0 \rho^{00}, \quad (33)$$

where $A_0 = (m^0/4\pi(d/2)^2\rho)$ is simply a constant related to the aerosol and monomer, such that d is the aerosol diameter, m^0 the monomer mass, and ρ their density (SESS17). The 0 superscript in the left-hand

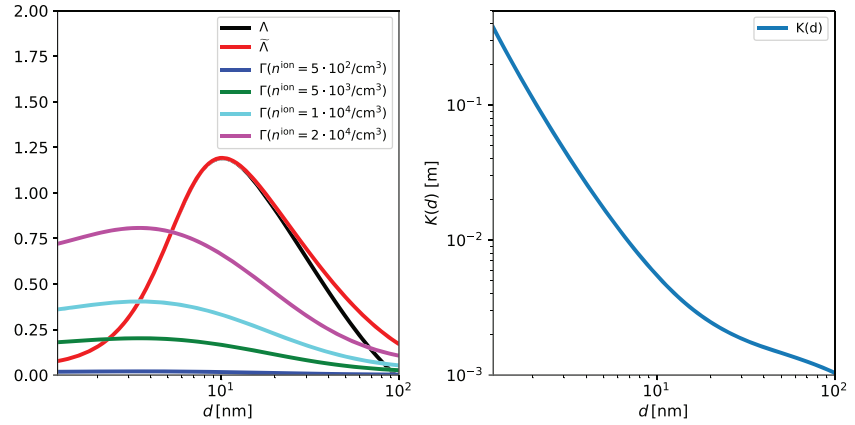


Figure 7. (left) The growth rate enhancement profiles associated with charged coagulation Λ and $\tilde{\Lambda}$, and ion condensation growth rate enhancement profiles Γ for ion concentrations n^{\pm} written in the legend. Note that all quantities are unitless. (right) $K(d)$ from Equation 42.

side (LHS) indicates that only neutral condensation is considered. In the presence of ions, the contribution to the condensation is presented in SESS17 as

$$GR_{\text{cond}}^{\pm} = A_0 n^0 \beta^{00} (1 + \Gamma), \quad (34)$$

where

$$\Gamma = 4 \left(\frac{n^{\pm}}{n^0} \right) \left(\frac{\beta^{\pm 0}}{\beta^{00}} \right) \left(\frac{m^{\pm}}{m^0} \right) \left(\frac{N^0(d)}{N^{\text{tot}}(d)} \right). \quad (35)$$

Γ is then the increase in growth rate caused by ion condensation relative to the neutral growth rate for pure neutral condensation. Positive and negative ions are treated symmetrically, such that interaction coefficients for the two species are $\beta^{+0} = \beta^{-0} = \beta^{\pm 0}$, $m^{+} = m^{-} = m^{\pm}$, and $n^{+} = n^{-} = n^{\pm}$. The final factor N^0/N^{tot} is given in Equation 31 assuming charge equilibrium. Note that all β are functions of aerosol diameter as shown in Figure 3. In Figure 7 on the left Γ can be seen for a charge equilibrated distribution of aerosols with sulfuric acid monomers $n^0 = 10^6 \text{ cm}^{-3}$, $m^0 = 100 \text{ AMU}$, and $m^{\pm} = 225 \text{ AMU}$ for a couple of ion-pair concentrations. As expected, Γ scales with n^{\pm} .

5.2. Coagulation Growth Rate

While the result of the condensation above is universally applicable to any aerosol distribution, a similar expression is harder to achieve for the coagulation, where aerosols of all diameters may coagulate with each other. Here we shall consider the growth rate of a monodisperse distribution for simplification and then compare with simulations that are reasonably approximated as such. From Equation 9 of Leppä et al. (2011), the growth rate of a monodisperse concentration N^T of completely neutral aerosols due to coagulation is

$$GR_{\text{coag}}^0 = \frac{d k^{00} N^T}{6}. \quad (36)$$

Here $k^{00}(d) = \kappa^{00}(d, d)$ is the neutral-neutral coagulation coefficient of particles at equal diameters. k^{00} is thus a function of diameter. Introducing ions, a fraction of the monodisperse aerosols will obtain a single charge. In this case, the growth rate from coagulation is

$$GR_{\text{coag}}^{\pm} = \frac{d}{3N^T} \left[\frac{1}{2} k^{00} (N^0)^2 + k^{0+} N^0 N^{+} + k^{0-} N^0 N^{-} + k^{+-} N^{+} N^{-} \right]. \quad (37)$$

As in the model, the terms with interactions between two positive aerosols and two negative aerosols have been neglected. Again, all coagulation coefficients k^{0+} , k^{0-} , and k^{+-} are functions of d , and now $N^T = N^0 + N^{+} + N^{-}$. If we assume that $k^{0\pm} = k^{0+} = k^{0-}$, and $N^{\pm} = N^{+} = N^{-}$, then

$$GR_{\text{coag}}^{\pm} = \frac{d}{3N^T} \left[\frac{1}{2} k^{00} (N^0)^2 + 2k^{0\pm} N^0 N^{\pm} + k^{+-} (N^{\pm})^2 \right] \quad (38)$$

$$= \frac{d k^{00} N^T}{6} \left[\left(\frac{N^0}{N^T} \right)^2 + 4 \frac{k^{0\pm}}{k^{00}} \left(\frac{N^\pm}{N^T} \frac{N^0}{N^T} \right) + 2 \frac{k^{+-}}{k^{00}} \left(\frac{N^\pm}{N^T} \right)^2 \right] \quad (39)$$

$$= \frac{d k^{00} N^T}{6} (1 + \Lambda), \quad (40)$$

where

$$(1 + \Lambda) = \left[\left(\frac{N^0}{N^T} \right)^2 + 4 \frac{k^{0\pm}}{k^{00}} \left(\frac{N^\pm}{N^T} \frac{N^0}{N^T} \right) + 2 \frac{k^{+-}}{k^{00}} \left(\frac{N^\pm}{N^T} \right)^2 \right]. \quad (41)$$

The relative concentrations of the $1 + \Lambda$ expression can be calculated based on Equation 31 assuming the aerosols to be in equilibrium with respect to their charge. Then Λ is independent of N^T and n^\pm . Thus, the GR from coagulation has a unitless and diameter-dependent adjustment $\Lambda(d)$ that is given by the coagulation coefficients and equilibrium charge fractions. Λ can be seen plotted in Figure 7 on the left. For $d > 100$ nm, Λ actually becomes slightly negative, since the assumption of like-charged coagulation is neglected. Including the like-charged terms in Equation 37 would produce an increase $\tilde{\Lambda}$ as seen in Figure 7, and for more advanced treatments multiple charge aerosol species could be included in the term. The fraction of multiply charged aerosols is, however, low for sizes below 100 nm, going from $\approx 1\%$ to $\approx 5\%$ between $d = 40$ nm and $d = 100$ nm (Hoppel & Frick, 1986). As multicharge aerosols are not handled by the model of the present work, we exclude it for consistency and direct comparison and use only Λ .

5.3. Growth Rate Increase From Ions

With expressions for the neutral and charged growth rate from condensation and coagulation in hand, we can consider two cases: (1) the growth rate due to both coagulation and condensation for a neutral monodisperse concentration N^T of aerosols and (2) the growth rate of the same concentration N^T of aerosols, however, with the presence of ions, condensing and charging a fraction of the aerosols. Taking the ratio of the two growth rates, we obtain a measure of the increase in growth rate due to the presence of charging ions on aerosols at diameter d and concentration N^T :

$$\begin{aligned} \Omega &= \frac{GR_{\text{cond}}^\pm + GR_{\text{coag}}^\pm}{GR_{\text{cond}}^0 + GR_{\text{coag}}^0} \\ &= \frac{K(d) \frac{n^0}{N^T} (1 + \Gamma) + 1 + \Lambda}{K(d) \frac{n^0}{N^T} + 1}, \end{aligned} \quad (42)$$

where $K(d) = \frac{6A_0(d)}{d} \frac{\beta^{00}(d)}{k^{00}(d)}$. $K(d)$ can be seen in Figure 7 and ranges from $\approx 10^{-2}$ at $d = 5$ nm to $\approx 10^{-3}$ at $d = 100$ nm.

To explore the regimes in which coagulation or condensation dominates the GR increase due to ions, we explore the limits of Equation 42. If we assume $N^T \ll K(d)n^0$, condensation is the dominant growth mechanism. Ω reduces to

$$\Omega = 1 + \Gamma. \quad (43)$$

On the other hand, if $N^T \gg K(d)n^0$, then the coagulation is the dominant growth mechanism and the expression reduces to

$$\Omega = 1 + \Lambda. \quad (44)$$

In the next subsection we simulate these two cases for appropriate atmospheric values, as well as cases in between, and compare with the equations above.

5.4. Growth Rates in Simulation

In order to calculate growth rates from the model, an initial number N^T of aerosols at $d = 1$ nm were grown in a loss-free environment with fixed sulfuric acid concentration n^0 and fixed ion concentration n^\pm , using parameters mentioned in section 3.6. As our goal is to compare model and theoretical results, two

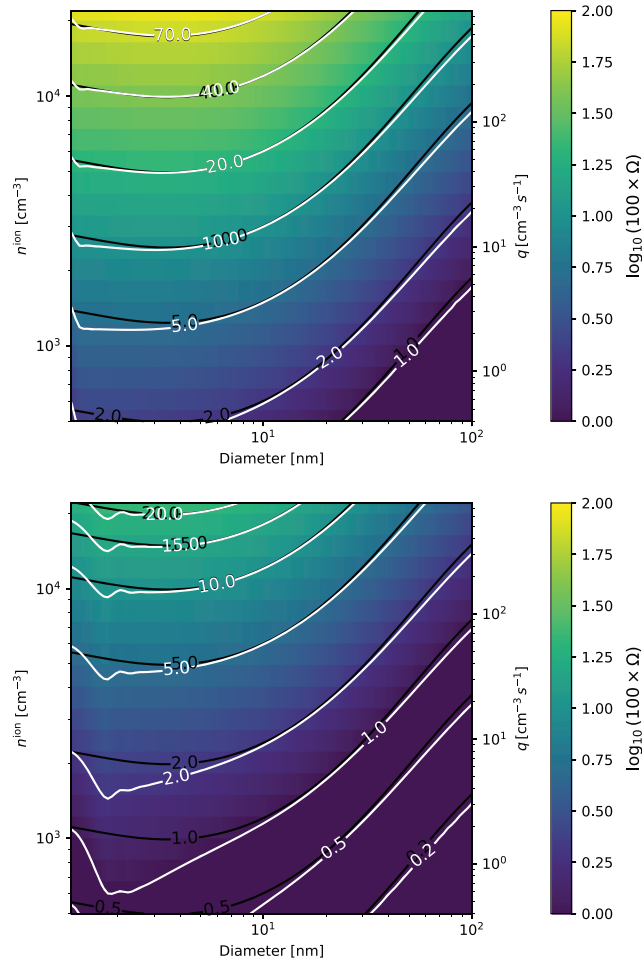


Figure 8. Charge enhancements of the growth rate Ω from condensation only. The black lines show the theoretical contours of Equation 42, in percent. The white lines show contours of simulated Ω in percent. The colors represent the logarithm of the same simulated Ω in percent. The y axis on the left-hand side of the panels shows the fixed ion-pair concentration, and the right-hand side shows the equivalent ion-pair production rate as calculated by $q = 1.6 \times 10^{-6} (n^{\pm})^2$ (top) Neutral monomer concentration $n^0 = 1 \times 10^6 \text{ cm}^{-3}$, equivalent to Figure 1 of SESS17. (bottom) $n^0 = 4 \times 10^6 \text{ cm}^{-3}$.

consideration must be made: (1) We focus on the simulation mean diameter rather than GR for the entire distribution, and (2) when considering coagulation we must take into consideration the fact that the number of aerosols N^T changes dynamically in each simulation depending on ambient conditions.

Since the model suffers from numerical diffusion as well as a broadening of the originally narrow distribution due to coagulation itself, the simulation quickly departs from the monodisperse initial conditions assumed above, so some extra care is needed to compare to the expressions in the previous subsection. At each point in time through each simulation we can calculate the mean aerosol volume in the simulation

$$\langle v \rangle = \frac{\sum_k N_k^T v_k}{\sum_k N_k^T}, \quad (45)$$

from which the mean diameter $\langle d \rangle$ is obtained. We can then consider the growth rate as

$$GR = \frac{d \langle d \rangle}{dt}. \quad (46)$$

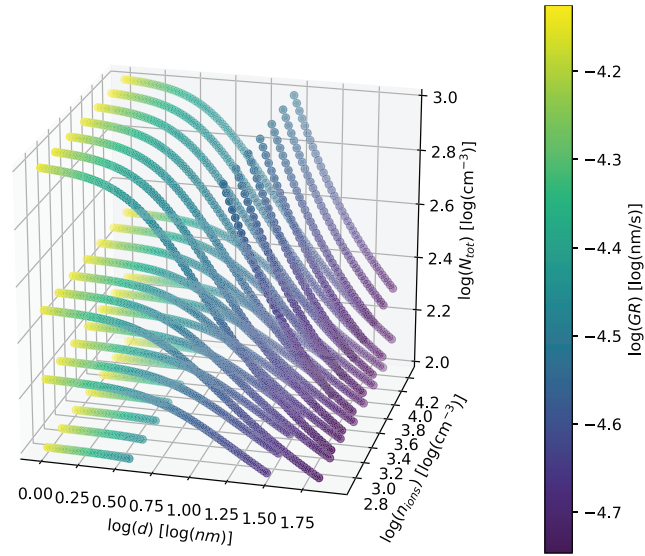


Figure 9. Subset of mean diameter growth rate enhancements in simulations at constant n^{ion} , including condensation and coagulation growth terms. As time evolves, N^T decreases and the mean diameter grows.

The equivalent number of aerosols at this diameter is simply N^T :

$$N^T = \frac{\sum_k N_k^T v_k}{\langle v \rangle} = \sum_k N_k^T. \quad (47)$$

Assuming $d = \langle d \rangle$ enables us to compare the simulated growth rate of the mean diameter to that of the analytical monodisperse distribution above. Then, we can produce simulated Ω by comparing the GR in simulations with similar N^T at similar $\langle d \rangle$ with and without ions present.

First, we focus on the condensation-only case of Equation 43, by decoupling the coagulation term from the model. Given a fixed ion-pair concentration n^\pm , an initially monodisperse distribution of $N^T = 1,000 \text{ cm}^{-3}$ was grown toward higher diameters. Growth rates of the mean diameter in simulations of 20 different levels of n^\pm were compared to the growth rate at the equivalent diameter of the neutral ($n^\pm = 0$) case for two levels of sulfuric acid $n^0 = 1 \times 10^6 \text{ cm}^{-3}$ and $n^0 = 4 \times 10^6 \text{ cm}^{-3}$. Both of these can be seen in Figure 8. The upper panel is equivalent to Figure 1 of SESS17. There is an excellent correspondence between the expression for $\Omega = 1 + \Gamma$ and the simulated GR enhancement in a coagulation free environment. Γ scales with n^\pm/n^0 , and by quadrupling n^0 from the top to the bottom panel in Figure 8, the effect is seen to be suppressed exactly with this factor in response. This is in effect the ion condensation effect.

Now, including also coagulation Equation 42 shows how Ω varies a function of d , n^\pm , n^0 , and N^T . Within the course of a single simulation, as the aerosols coagulate N^T decreases, which in turn reduces the effect of coagulation. It is convenient to be able to compare growth rates at similar N^T while varying d , n^\pm , and n^0 . Therefore, given an ion-pair concentration n^\pm , 20 simulations of initial N^T aerosols between 10^2 and 10^8 cm^{-3} were computed. Then, even though N^T decreases with time within a single simulation, the growth rate of the mean diameter at concentration N^T could be interpolated between simulations. We assume a value of $n^0 = 10^6 \text{ cm}^{-3}$, and for around 20 values of n^\pm between 0 and $22,005 \text{ cm}^{-3}$ we allow aerosols at 1.1 nm and different initial concentrations to coagulate, condensate, and interact with ions. For each simulation, the growth rate $GR(\langle d \rangle)$ and total aerosol concentration $N^T(\langle d \rangle)$ of the mean diameter $\langle d \rangle$ are obtained. A subset of the simulation growth rates are seen in Figure 9. The trajectory of $\langle d \rangle$ in this space for a single simulation can be seen as beginning at the lowest value of $\langle d \rangle$, for an initial N^T , and growing toward higher values as time progresses while N^T decreases.

Interpolating in this space for two constant values of N^T yields the two panels of Figure 10. Here, the added effects of ions on the coagulation and condensation, that is, Λ and Γ , are comparable in magnitude. As can be seen when comparing the pure condensation in Figure 8 and pure coagulation contained in Λ of

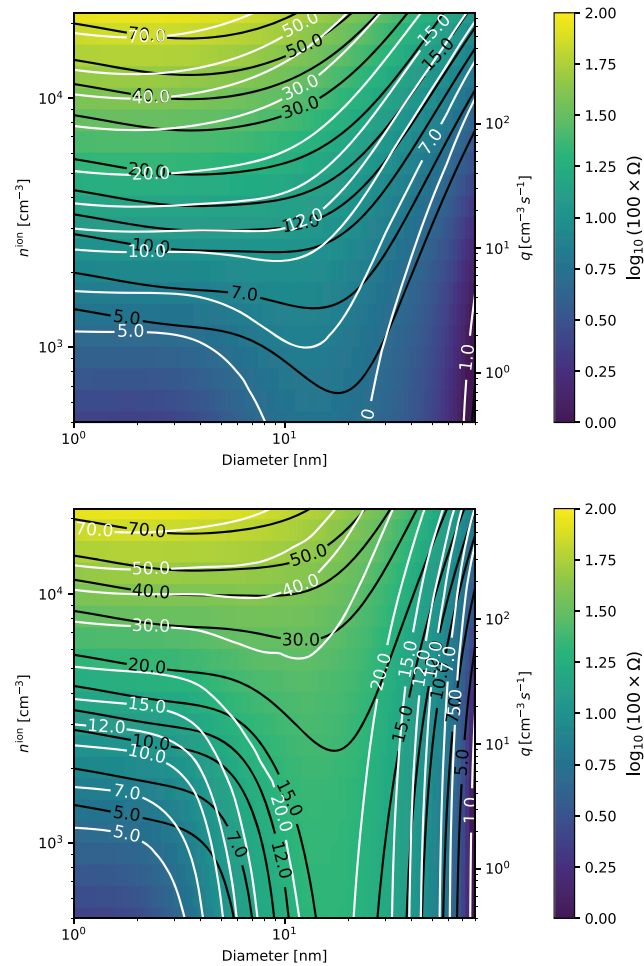


Figure 10. Charge enhancements of the growth rate Ω from condensation and coagulation. The black lines show the theoretical contours of Equation 42, in percent. The white lines show contours of simulated Ω in percent. Both panels are calculated from a horizontal slice through the data of Figure 9. The y axis on the left-hand side of the panels shows the fixed ion-pair concentration, and the right-hand side shows the equivalent ion-pair production rate as calculated by $q = 1.6 \times 10^{-6}(n^{\pm})^2$. (top) Total particle concentration $N^T = 100 \text{ cm}^{-3}$. (bottom) $N^T = 500 \text{ cm}^{-3}$.

Figure 7 with Figure 10, we can identify the two components that contribute to the charged growth rate enhancement. Ion-induced condensation enhances growth rates for increasing n^{\pm} and small diameters, that is, the bulge in the upper left corners. Added growth from charged coagulation via Λ manifests itself as an increase with diameter, followed by a decreases back to uncharged growth as coagulation coefficients for single-charge aerosols and neutral aerosols tend to be equal for very large diameters. This corresponds to the vertical band across the two figures. The coagulation effect is independent of n^{\pm} , as expected when aerosols are in a charged fraction equilibrium. In the top panel, a constant value of $N^T = 100 \text{ cm}^{-3}$ is depicted. In the bottom panel, $N^T = 500 \text{ cm}^{-3}$, and as expected, the contribution to Ω from coagulation at the higher total particle concentration is stronger while the condensation of ions remains the same. There is a good but not 1-to-1 correspondence between the simulated and theoretical contours in the two figures; however, the principal behavior of theory and simulation is the same.

Holding instead n^{\pm} as constant and using vertical slices along the d direction of Figure 9 allows for the calculation of the data in Figure 11. In comparison to Figure 10 N^T is now varied instead of n^{\pm} . As N^T increases, coagulation and therefore Λ become progressively more dominant for Ω . Increasing n^{\pm} from the top panel to the bottom panel makes the Γ ion condensation term contribute more to Ω for the lower diameter aerosols, on par with the theoretical Γ .

It should be noted that in general, ion mass, concentrations, and interaction coefficients can be set and calculated individually, in the code, and need not to be restricted to the symmetric case tested here.

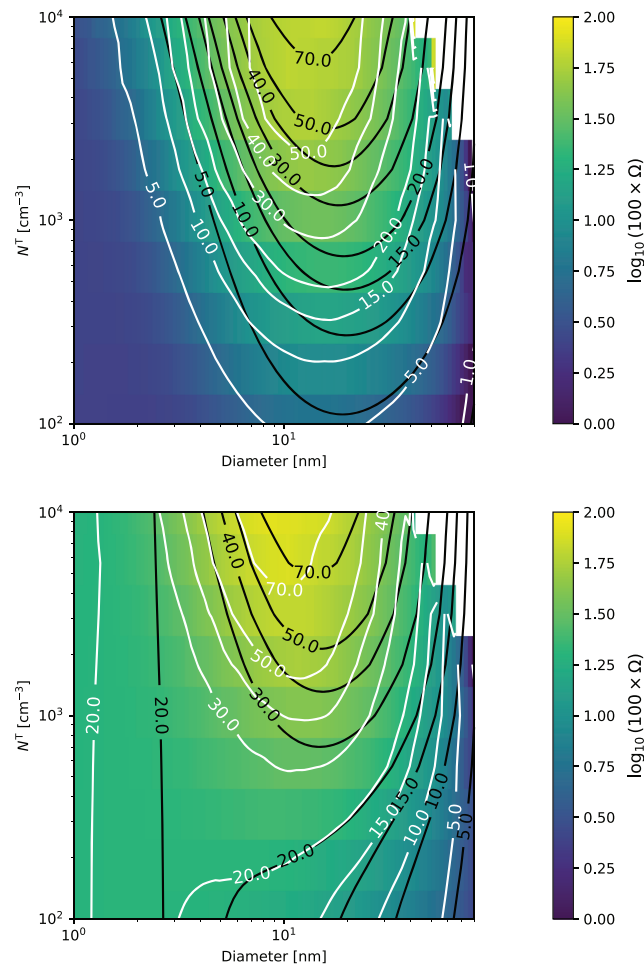


Figure 11. Charge enhancements of the growth rate Ω from condensation and coagulation, with a constant n^{ion} . The black lines show the theoretical contours of Equation 42, in percent. The white lines show contours of simulated Ω in percent. Both panels are calculated from a vertical slice through the data of Figure 9. (top) Ion-pair concentration $n^{\pm} = 500 \text{ cm}^{-3}$. (bottom) $n^{\pm} = 5,000 \text{ cm}^{-3}$.

6. Discussion and Conclusion

In the present work a numeric model for simulating aerosol growth in the presence of charge has been developed and presented. The code consists of a zero-dimensional time integration model, where the interactions between ions and (charged) aerosols are taken into account. In particular, ions are treated as massive condensing particles contributing to the growth rate in an implementation similar to condensation of neutral clusters here modeled as (H_2SO_4), while accounting for their inherent transfer of charge. The model is then used to investigate the newly demonstrated effect of ion-induced condensation from H. Svensmark et al. (2017) and a good agreement between model output and the theoretical and experimental SESS17 results is demonstrated employing condensation-only assumptions. Once coagulation is taken into account, we explore the conditions under which ion condensation is relevant and show that while coagulation adds to the growth rate of aerosols when ions are present, it is not dependent on ion concentration, and in this sense the ion condensation contribution to growth rate can be said to function independent of coagulation. Naturally in both experimental and real atmosphere scenarios there will be growth due to coagulation when the aerosol distribution is not well approximated by monodisperse conditions, there will be loss mechanisms and temporally varying concentrations of the ion pairs and neutral clusters from which aerosols grow in size. Furthermore, the positive and negative ions may in general be of different masses. These are parameters and dynamics that may be handled by the model in its current implementation.

The concept of ion-induced condensation is still new, and further investigation into its dynamics and implications is needed. The present model may prove a useful tool for describing the mechanism under a range on conditions and parameters relevant for the atmosphere, including some that would otherwise be unobtainable in the laboratory. While we have done a step toward describing it in the context of aerosol coagulation, more detailed work remains for future studies. Here, various scenarios could be considered such the effect on ion-induced condensation of introducing losses to experiment walls or large preexisting aerosols. Simulations of realistic new particle formation events should be studied, to examine if the growth rate is enhanced under such scenarios. For atmospheric relevance it is necessary transform the effect of the ion condensation on the growth rate to a survival probability of the particles, that is, to estimate the change in the number of CCN. This can be done either by numerical modeling or a simple theoretical estimate (Kürten et al., 2015; Lehtinen et al., 2007). Also, the simulations depicted in Figure 8 could be repeated for upper tropospheric conditions with high ion-pair production rates, low temperatures, and low pressure. Furthermore, an implementation of ion condensation into in higher-dimensional models, that is, atmospheric circulation models would. Here, the current model would meet at challenge as numerical diffusion from the condensation term and computational weight of the coagulation term would need to be optimized.

The model could also be expanded to include more or different cluster-species. This could be relevant for investigating, for instance, how these species affect the growth of aerosols such as the role of organics in early aerosol growth (Tröstl et al., 2016). Implementing evaporation of small clusters would allow for the model to be used in nucleation studies, as well for systems relevant to Earth (R. Zhang et al., 2004) or more exotic systems like TiO_2 relevant to brown dwarfs or exoplanets (Lee et al., 2015). Furthermore, the model may provide insight into the fast dust grain growth observed in supernovae remnants (Bevan et al., 2017; Gall et al., 2014) and in high redshift galaxies (Michałowski, 2015; Watson et al., 2015).

Appendix A: Interaction Parameters Between Particles

Here the parameters of the model are defined. We note that the calculated enhancement factors and potentials are system specific and that the calculations presented here should be considered as a first approximation.

A1. Brownian Coagulation Kernel

The interaction coefficient between two aerosols in the Brownian regime is given by Jacobson and Seinfeld (2004) as

$$\beta_{i,j}^B = \frac{4\pi(a_i + a_j)(D_{m,i} + D_{m,j})}{\frac{a_i + a_j}{a_i + a_j + (\delta_{m,i} + \delta_{m,j})^{1/2}} + \frac{4(D_{m,i} + D_{m,j})}{\sqrt{\bar{v}_i^2 + \bar{v}_j^2}(a_i + a_j)}} V_{i,j}, \quad (\text{A1})$$

where a_i and a_j are the radii of the two interacting particles. $\bar{v}_i = \sqrt{8k_B T / (\pi M_i)}$ is the average speed of the aerosol, with M_i being the mass of the aerosol. $D_{m,i}$ is the diffusion constant of particle of radius a_i :

$$D_{m,i} = \frac{k_B T}{6\pi a_i \eta} [1 + \text{Kn}_i (A_m + B_m \exp(-C_m / \text{Kn}_i))], \quad (\text{A2})$$

where the Knudsen number is given by $\text{Kn}_i = \lambda / a_i$ and where λ is the mean free path of an air molecule. η is the dynamic viscosity of air and

$$\delta_i = \frac{(2a_i + \lambda_i)^3 - (4a_i^2 + \lambda_i^2)^{3/2}}{6a_i \lambda_i} - 2a_i. \quad (\text{A3})$$

The three constants in the diffusion term are quoted by (Kasten, 1968) as

$$\begin{aligned} A_m &= 1.249, \\ B_m &= 0.42, \\ C_m &= 0.87. \end{aligned}$$

Finally the $V_{i,j}$ is an enhancement factor that can take interactions between the aerosols into account. This term will be defined in the next section.

A2. Calculation of Enhancement Factors for Coagulation of Charged Ions

In the case of charged aerosols, the Brownian coagulation coefficients should be corrected since their charge as well as their subsequent induction of additional charge results in a modified potential. For any potential, the correction factor for aerosols in the continuum regime ($Kn \rightarrow 0$) of radii a_i and a_j is (Jacobson & Seinfeld, 2004),

$$W_{i,j}^c = \frac{1}{(a_i + a_j) \int_{a_i+a_j}^{\infty} D_{\infty}/D_{i,j} \exp \left[\frac{E_{i,j}(r)}{k_B T} \right] r^{-2} dr}, \quad (A4)$$

where $E_{i,j}(r)$ is the interaction potential between the two aerosols at separation r , k_B is the Boltzmann constant, and T is the temperature. Viscous forces are taken into account by the following expression:

$$D_{\infty}/D_{i,j} = 1 + \frac{2.6 a_i a_j}{(a_i + a_j)^2} \sqrt{\frac{a_i a_j}{(a_i + a_j)(r - a_i - a_j)}} + \frac{a_i a_j}{(a_i + a_j)(r - a_i - a_j)}. \quad (A5)$$

In the kinetic regime ($Kn \rightarrow \infty$) when the interaction between the two aerosols is attractive and has a singularity at contact, the enhancement factor is (Marlow, 1980)

$$W_{i,j}^k = \frac{-1}{2(a_i + a_j)^2 k_B T} \int_{a_i+a_j}^{\infty} \left(\frac{dE_{i,j}}{dr} + r \frac{d^2 E_{i,j}}{dr^2} \right) \exp \left[\frac{-1}{k_B T} \left(\frac{r}{2} \frac{dE_{i,j}}{dr} + E_{i,j} \right) \right] r^2 dr. \quad (A6)$$

A3. The Potentials

In the present work the aerosols can be charged with a single charge, either positive or negative. Since the aerosols are made of dielectric medium the charge interaction will involve mirror charges, and the interaction potential will be slightly more involved. The potential representation used here is based on Bichoutskaia et al. (2010) for two spheres of radii a_i and a_j . For the two spheres with charge Q_i and Q_j , permittivity ϵ_i and ϵ_j , and at a central distance r ,

$$E_{EM,i,j}(r) = K \frac{Q_i Q_j}{r} - Q_i \sum_{m=1}^{\infty} \sum_{l=0}^{\infty} \frac{(k_j - 1)m}{(k_j + 1)m + 1} \frac{(l + m)!}{l!m!} \times \frac{a_j^{2m+1}}{r^{2m+l+2}} A_{1,l} - \frac{1}{K} \sum_{l=1}^{\infty} \frac{(k_i + 1)l + 1}{(k_i - 1)l} \frac{A_{1,l} A_{1,l}}{a_i} \frac{2l+1}{i}, \quad (A7)$$

where $K = 1/4\pi\epsilon_0 \approx 9 \times 10^9$ Vm/C, $k_i = \epsilon_i/\epsilon_0$ and $k_j = \epsilon_j/\epsilon_0$ and $A_{1,l}$ are the coefficients found by solving the following implicit system of linear equations:

$$A_{1,l} = a_i V_i \delta_{l,0} - \frac{(k_i - 1)l}{(k_i + 1)l + 1} \frac{a_i^{2l+1}}{r^{l+1}} a_j V_j + \frac{(k_i - 1)l}{(k_i + 1)l + 1} \times \sum_{l_2=0}^{\infty} \sum_{l_3=0}^{\infty} \frac{(k_j - 1)l_2}{(k_j + 1)l_2 + 1} \frac{(l + l_2)!}{l!l_2!} \frac{(l_2 + l_3)!}{l_2!l_3!} \times \frac{a_i^{2l+1} a_j^{2l_2+1}}{r^{l+2l_2+l_3+2}} A_{1,l_3}. \quad (A8)$$

Here $a_i V_i = KQ_i$, $a_j V_j = KQ_j$, and $\delta_{l,0}$ are the Kronecker delta function.

In addition to the electrostatic potential, it is assumed that there are short range van der Waals forces present. This potential will ensure that there is a singular potential at contact and make the expression for the kinetic enhancement factor valid (Marlow, 1980). The van der Waals potential is given by

$$E_{vdw,i,j}(r) = -\frac{A}{6} \left[\frac{2a_i a_j}{r^2 - (a_i + a_j)^2} + \frac{2a_i a_j}{r^2 - (a_i - a_j)^2} + \log \left(\frac{r^2 - (a_i + a_j)^2}{r^2 - (a_i - a_j)^2} \right) \right]. \quad (A9)$$

Here A is the Hamaker constant measured to be $A = (6.4 \pm 2.6)10^{-20}$ J for H_2SO_4 - H_2O aerosol interactions at 300 K (Chan & Mozurkewich, 2001).

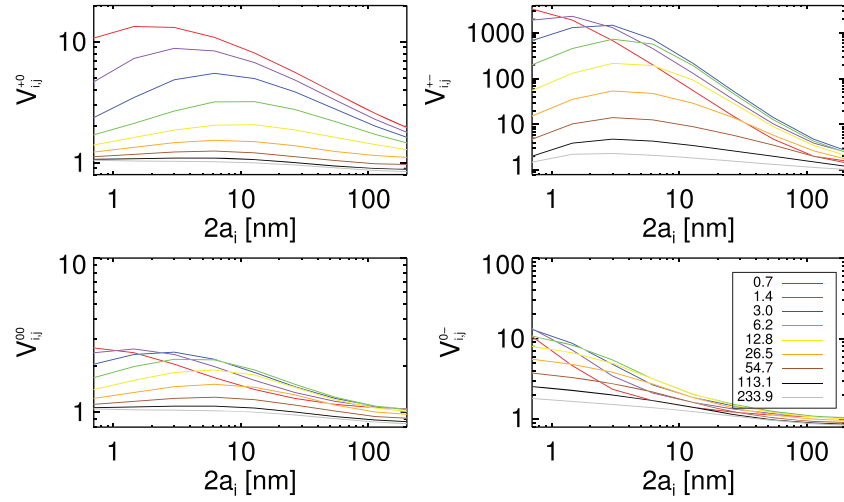


Figure A1. Enhancement factors between a particle of size a_i and a_j due to all effects mentioned in Appendix A1 and for $T = 300$ K, $\eta = 1.8362 \times 10^{-5}$ kg m $^{-1}$ s $^{-1}$, and mean free path $\lambda = 65$ nm, for different charges on each of the coagulating spheres. Numbers in the legend are diameters in units of nm.

A4. Connecting the Continuum Regime With the Kinetic Regime

Calculation of $W_{i,j}^c$ and $W_{i,j}^k$ must be done numerically, and it is therefore convenient to make the following variable transformation:

$$x = \frac{a_i + a_j}{r}. \quad (\text{A10})$$

The interval of integration is changed from $[a_i + a_j; \infty[$ to $[0; 1]$, so that the enhancement factor in the continuum limit becomes

$$W_{i,j}^c = \left(\int_0^1 D_{\infty}/D_{i,j} \exp \left[\frac{E_{i,j}((a_i + a_j)/x)}{k_B T} \right] dx \right)^{-1}, \quad (\text{A11})$$

while the enhancement factor in the kinetic limit becomes

$$W_{i,j}^k = \frac{-1}{2k_B T} \int_0^1 \frac{1}{x^2} \left(x \frac{d^2 E_{i,j}}{dx^2} - \frac{dE_{i,j}}{dx} \right) \exp \left[\frac{-1}{k_B T} \left(E_{i,j} - \frac{x}{2} \frac{dE_{i,j}}{dx} \right) \right] dx. \quad (\text{A12})$$

The potential used here is

$$E_{i,j} = E_{EM,i,j} + E_{vdW,i,j}. \quad (\text{A13})$$

Finally, the correction factor that interpolates between the continuum and kinetic regime is given by Alam (1987):

$$V_{i,j} = \frac{W_{i,j}^c [1 + 4(D_{m,i} + D_{m,j})/\sqrt{v_i^2 + v_j^2}(a_i + a_j)]}{1 + (W_{i,j}^c/W_{i,j}^k)(4(D_{m,i} + D_{m,j})/\sqrt{v_i^2 + v_j^2}(a_i + a_j))}. \quad (\text{A14})$$

Figure A1 graphically displays the calculated enhancement factors.

The above Brownian coagulation kernel can be used as a basis for including electrostatic and van der Waals forces. Such effects are conveniently included by multiplying the Brownian coagulation kernel by a correction or enhancement factor. Such that

$$\begin{aligned} \kappa_{i,j}^{+0} &= \beta_{i,j}^B V_{i,j}^{+0}, \\ \kappa_{i,j}^{00} &= \beta_{i,j}^B V_{i,j}^{00}, \\ \kappa_{i,j}^{0-} &= \beta_{i,j}^B V_{i,j}^{0-}. \end{aligned}$$

The above calculations do not include three-body interactions such as discussed in López-Yglesias and Flanagan (2013), where charged aerosols are slowed down by collisions with (but not attachments to) a third body, and subsequently attached to another aerosol of a given charge. This will be important in the recombination between small ion pairs, and that is the likely reason that the $V_{i,j}^{+-}$ coefficients for the smallest particles do not reach the experimentally determined recombination coefficient $\alpha = 1.6 \times 10^{-6} \text{ cm}^3 \text{ s}^{-1}$ but is a factor ≈ 5 too low. We correct this by simple adjustment, to obtain the final coagulation coefficients:

$$\kappa_{i,j}^{+-} = \frac{\beta_{i,j}^B V_{i,j}^{+-}}{1 + \left(\frac{\beta_{i,j}^B V_{i,j}^{+-}}{\alpha} - 1 \right) \exp \left(-\frac{\sqrt{d_i^2 + d_j^2}}{d_s} \right)}, \quad (\text{A15})$$

where $d_s = 100 \text{ nm}$ is a characteristic scale length. The condensation coefficients used in the condensation equations are

$$\begin{aligned} \beta_k^{00} &= \beta_{0,k}^B V_{0,k}^{00}, \\ \beta_k^{0+} &= \beta_{0,k}^B V_{0,k}^{0+}, \\ \beta_k^{0-} &= \beta_{0,k}^B V_{0,k}^{0-}, \\ \beta_k^{+0} &= \beta_{+,k}^B V_{+,k}^{+0}, \\ \beta_k^{-0} &= \beta_{-,k}^B V_{-,k}^{-0}. \end{aligned} \quad (\text{A16})$$

Note that these β only have one index k for the radius of the aerosol a_k , as the radius of the condensing monomers (denoted with subscripts 0, −, and +) are fixed at radii a_0 , a_- , and a_+ . Again, the recombination coefficient is used as a limit for the final two terms:

$$\beta_k^{++} = \frac{\beta_{-,k}^B V_{i,j}^{-+}}{1 + \left(\frac{\beta_{-,k}^B V_{i,j}^{-+}}{\alpha} - 1 \right) \exp \left(-\frac{a_j}{a_s} \right)}, \quad (\text{A17})$$

$$\beta_k^{+-} = \frac{\beta_{+,k}^B V_{i,j}^{+-}}{1 + \left(\frac{\beta_{+,k}^B V_{i,j}^{+-}}{\alpha} - 1 \right) \exp \left(-\frac{a_j}{a_s} \right)}, \quad (\text{A18})$$

where $\alpha = 1.6 \times 10^{-6} \text{ cm}^3 \text{ s}^{-1}$.

Data Availability Statement

All aerosol simulation data in this work are produced using the ION-CAGE v1.0 code described in the main text and interaction coefficients described in Appendix A1. Both are available through a Zenodo repository (Svensmark, <https://doi.org/10.5281/zenodo.3931374>), and all results can be reproduced using parameters stated in the main text.

Acknowledgments

J. S. is funded by the Danish council for independent research under the project “Fundamentals of Dark Matter Structures”, DFF-6108-00470. N. J. S. wishes to thank the generous support of the Israeli Ministry of Energy, Grant 218-11-036. J. S. thanks Caroline Richardt Beck for illustration design assistance and Asbjørn Jacobsen for identifying typos in two equations.

References

- Alam, M. K. (1987). The effect of van der Waals and viscous forces on aerosol coagulation. *Aerosol Science and Technology*, 6(1), 41–52. <https://doi.org/10.1080/02786828708959118>
- Bevan, A., Barlow, M. J., & Milisavljevic, D. (2017). Dust masses for SN 1980K, SN1993J and Cassiopeia A from red-blue emission line asymmetries. *Monthly Notices of the RAS*, 465, 4044–4056. <https://doi.org/10.1093/mnras/stw2985>
- Bichoutskaia, E., Boatwright, A. L., Khachatourian, A., & Stace, A. J. (2010). Electrostatic analysis of the interactions between charged particles of dielectric materials. *The Journal of Chemical Physics*, 133(2), 024105. <https://doi.org/10.1063/1.3457157>
- Chan, T. W., & Mozurkewich, M. (2001). Measurement of the coagulation rate constant for sulfuric acid particles as a function of particle size using tandem differential mobility analysis. *Journal of Aerosol Science*, 32(3), 321–339. [https://doi.org/10.1016/S0021-8502\(00\)00081-1](https://doi.org/10.1016/S0021-8502(00)00081-1)
- Dunne, E. M., Gordon, H., Kürten, A., Almeida, J., Duplissy, J., Williamson, C., et al. (2016). Global atmospheric particle formation from CERN CLOUD measurements. *Science*, 354(6316), 1119–1124. <https://doi.org/10.1126/science.aaf2649>
- Enghoff, M. B., & Svensmark, J. (2017). Measurement of the charging state of 4–70 nm aerosols. *Journal of Aerosol Science*, 114(Supplement C), 13–20. <https://doi.org/10.1016/j.jaerosci.2017.08.009>
- Fehlberg, E. (1969). Low-order classical Runge-Kutta formulas with stepsize control and their application to some heat transfer problems: National Aeronautics and Space Administration.
- Gall, C., Hjorth, J., Watson, D., Dwek, E., Maund, J. R., Fox, O., et al. (2014). Rapid formation of large dust grains in the luminous supernova 2010jl. *Nature*, 511, 326–329. <https://doi.org/10.1038/nature13558>

- Hoppel, W. A. (1985). Ion aerosol attachment coefficients, ion depletion, and the charge distribution on aerosols. *Journal of Geophysical Research*, 90(D4), 5917–5923. <https://doi.org/10.1029/JD090iD04p05917>
- Hoppel, W. A., & Frick, G. M. (1986). Ion-aerosol attachment coefficients and the steady-state charge distribution on aerosols in a bipolar ion environment. *Aerosol Science and Technology*, 5(1), 1–21. <https://doi.org/10.1080/02786828608959073>
- Jacobson, M. Z. (2005). *Fundamentals of atmospheric modeling*. Cambridge: Cambridge University Press.
- Jacobson, M. Z., & Seinfeld, J. H. (2004). Evolution of nanoparticle size and mixing state near the point of emission. *Atmospheric Environment*, 38, 1839–1850. <https://doi.org/10.1016/j.atmosenv.2004.01.014>
- Kasten, F. (1968). Falling speed of aerosol particles. *Journal of Applied Meteorology*, 7(5), 944–947. [https://doi.org/10.1175/1520-0450\(1968\)007<0944:FSOAP>2.0.CO;2](https://doi.org/10.1175/1520-0450(1968)007<0944:FSOAP>2.0.CO;2)
- Kazil, J., & Lovejoy, E. R. (2004). Tropospheric ionization and aerosol production: A model study. *Journal of Geophysical Research*, 109, D19206. <https://doi.org/10.1029/2004JD004852>
- Kürten, A., Williamson, C., Almeida, J., Kirkby, J., & Curtius, J. (2015). On the derivation of particle nucleation rates from experimental formation rates. *Atmospheric Chemistry and Physics*, 15(8), 4063–4075. <https://doi.org/10.5194/acp-15-4063-2015>
- Laakso, L., Mäkelä, J. M., Pirjola, L., & Kulmala, M. (2002). Model studies on ion-induced nucleation in the atmosphere. *Journal of Geophysical Research*, 107(D20), 4427–4445. <https://doi.org/10.1029/2002JD002140>
- Lee, G., Helling, C., Giles, H., & Bromley, S. T. (2015). Dust in brown dwarfs and extra-solar planets IV. Assessing TiO₂ and SiO nucleation for cloud formation modelling. *Astronomy & Astrophysics*, 575, A11. <https://doi.org/10.1051/0004-6361/201424621>
- Lehtinen, K. E. J., Maso, M. D., Kulmala, M., & Kerminen, V.-M. (2007). Estimating nucleation rates from apparent particle formation rates and vice versa: Revised formulation of the kerminen-kulmala equation. *Journal of Aerosol Science*, 38(9), 988–994. <https://doi.org/10.1016/j.jaerosci.2007.06.009>
- Leppä, J., Anttila, T., Kerminen, V.-M., Kulmala, M. E. J., & Lehtinen, K. (2011). Atmospheric new particle formation: Real and apparent growth of neutral and charged particles. *Atmospheric Chemistry and Physics*, 11, 4939–4955. <https://doi.org/10.5194/acp-11-4939-2011>
- Leppä, J., Kerminen, V.-M., Laakso, L., Korhonen, H., Lehtinen, K. E. J., Gagne, S., et al. (2009). Ion-UHMA: A model for simulating the dynamics of neutral and charged aerosol particles. *Boreal Environment Research*, 14, 559–575.
- López-Yglesias, X., & Flagan, R. C. (2013). Ion-aerosol flux coefficients and the steady-state charge distribution of aerosols in a bipolar ion environment. *Aerosol Science and Technology*, 47(6), 688–704. <https://doi.org/10.1080/02786826.2013.783684>
- Määttänen, A., Merikanto, J., Henschel, H., Duplissy, J., Makkonen, R., Ortega, I. K., & Vehkamäki, H. (2018). New parameterizations for neutral and ion-induced sulfuric acid-water particle formation in nucleation and kinetic regimes. *Journal of Geophysical Research: Atmospheres*, 123, 1269–1296. <https://doi.org/10.1002/2017JD027429>
- Marlow, W. H. (1980). Derivation of aerosol collision rates for singular attractive contact potentials. *The Journal of Chemical Physics*, 73(12), 6284–6287. <https://doi.org/10.1063/1.440126>
- McGrath, M. J., Olenius, T., Ortega, I. K., Loukonen, V., Paasonen, P., Kurtén, T., et al. (2012). Atmospheric Cluster Dynamics Code: A flexible method for solution of the birth-death equations. *Atmospheric Chemistry and Physics*, 12(5), 2345–2355. <https://doi.org/10.5194/acp-12-2345-2012>
- Michalowski, M. J. (2015). Dust production 680–850 million years after the Big Bang. *Astronomy and Astrophysics*, 577, A80. <https://doi.org/10.1051/0004-6361/201525644>
- Pierce, J. R., & Adams, P. J. (2009). Can cosmic rays affect cloud condensation nuclei by altering new particle formation rates? *Geophysical Research Letters*, 36, L09820. <https://doi.org/10.1029/2009GL037946>
- Prakash, A., Bapat, A. P., & Zachariah, M. R. (2003). A simple numerical algorithm and software for solution of nucleation, surface growth, and coagulation problems. *Aerosol Science and Technology*, 37(11), 892–898. <https://doi.org/10.1080/02786820300933>
- Seigneur, C., Hudischewskyj, A. B., Seinfeld, J. H., Whitby, K. T., Whitby, E. R., Brock, J. R., & Barnes, H. M. (1986). Simulation of aerosol dynamics: A comparative review of mathematical models. *Aerosol Science and Technology*, 5(2), 205–222. <https://doi.org/10.1080/02786828608959088>
- Seinfeld, J. H., & Pandis, S. N. (2006). *Atmospheric chemistry and physics: From air pollution to climate change* (2nd ed.). United States: John Wiley & Sons, Inc.
- Shampine, L. F., Watts, H. A., & Davenport, S. M. (1976). Solving nonstiff ordinary differential equations the state of the art. *SIAM Review*, 18(3), 376–411. <https://doi.org/10.1137/1018075>
- Svensmark, H., Enghoff, M. B., & Pedersen, J. O. P. (2013). Response of cloud condensation nuclei (> 50 nm) to changes in ion-nucleation. *Physics Letters A*, 377(37), 2343–2347. <https://doi.org/10.1016/j.physleta.2013.07.004>
- Svensmark, H., Enghoff, M. B., Shaviv, N. J., & Svensmark, J. (2017). Increased ionization supports growth of aerosols into cloud condensation nuclei. *Nature Communications*, 8(1), 2199. <https://doi.org/10.1038/s41467-017-02082-2>
- Svensmark, J. Ion-cage. <https://doi.org/10.5281/zenodo.3931374>
- Tröstl, J., Chuang, W. K., Gordon, H., Heinritzi, M., Yan, C., Molteni, U., et al. (2016). The role of low-volatility organic compounds in initial particle growth in the atmosphere. *Nature*, 533(7604), 527–531. <https://doi.org/10.1038/nature18271>
- Watson, D., Christensen, L., Knudsen, K. K., Richard, J., Gallazzi, A., & Michalowski, M. J. (2015). A dusty, normal galaxy in the epoch of reionization. *Nature*, 519, 327–330. <https://doi.org/10.1038/nature14164>
- Wiedensohler, A. (1988). An approximation of the bipolar charge distribution for particles in the submicron size range. *Journal of Aerosol Science*, 19(3), 387–389. [https://doi.org/10.1016/0021-8502\(88\)90278-9](https://doi.org/10.1016/0021-8502(88)90278-9)
- Yu, F. (2010). Ion-mediated nucleation in the atmosphere: Key controlling parameters, implications, and look-up table. *Journal of Geophysical Research*, 115, D03206. <https://doi.org/10.1029/2009JD012630>
- Yu, F., & Turco, R. P. (2001). From molecular clusters to nanoparticles: Role of ambient ionization in tropospheric aerosol formation. *Journal of Geophysical Research*, 106(D5), 4797–4814. <https://doi.org/10.1029/2000JD900539>
- Zhang, Y., Seigneur, C., Seinfeld, J. H., Jacobson, M. Z., & Binkowski, F. S. (1999). Simulation of aerosol dynamics: A comparative review of algorithms used in air quality models. *Aerosol Science and Technology*, 31(6), 487–514. <https://doi.org/10.1080/027868299304039>
- Zhang, R., Suh, I., Zhao, J., Zhang, D., Fortner, E. C., Tie, X. X., et al. (2004). Atmospheric new particle formation enhanced by organic acids. *Science*, 304(5676), 1487–1490. <https://doi.org/10.1126/science.1095139>